Original Article

Nanoassemblies loaded with low-dose paclitaxel can enhance the response of lung cancer immunotherapy by activating dendritic cells

Jianlin Long[1#^], Dairong Li[1#], Wei Zhao[2#], Guanzhong Liang[1], Lumi Huang[1], Shuangyi Lei[1], Yan Li[1]

[1]Department of Medical Oncology, Chongqing University Cancer Hospital & Chongqing Cancer Institute & Chongqing Cancer Hospital, Chongqing, China; [2]Oncology Radiotherapy Center, Chongqing University Cancer Hospital & Chongqing Cancer Institute & Chongqing Cancer Hospital, Chongqing, China

Contributions: (I) Conception and design: J Long, D Li; (II) Administrative support: J Long, D Li; (III) Provision of study materials or patients: W Zhao, Y Li; (IV) Collection and assembly of data: W Zhao, G Liang, L Huang, S Lei; (V) Data analysis and interpretation: W Zhao, G Liang, L Huang, S Lei; (VI) Manuscript writing: All authors; (VII) Final approval of manuscript: All authors.

[#]These authors contributed equally to this work.

Correspondence to: Jianlin Long, MD. Department of Medical Oncology, Chongqing University Cancer Hospital & Chongqing Cancer Institute & Chongqing Cancer Hospital, No. 181 Hanyu Road, Shapingba District, Chongqing 400030, China. Email: jianlin_long@163.com.

Background: The immune tolerance of the tumor immune microenvironment (TIME) restricts the response to immune checkpoint inhibitors (ICIs). Targeted activation of dendritic cells (DCs) in the TIME seems to be a scheme for improving the therapeutic effect of ICIs treatment. The purpose of this study was to utilize nanotechnology to reprogram the immunosuppressive tumor immune microenvironment *in situ*, improving the response of ICIs to lung cancer.

Methods: In this study, a folic acid (FA)-modified nanoassembly (NA) loaded with low-dose paclitaxel (PTX) (FA-PTX NA), self-assembled by distearoylphosphatidylethanolamine-methoxy polyethylene glycol 2000-folic acid (DSPE-mPEG2000-FA) and PTX, was designed to reprogram the DC function of the TIME to sensitize cells to cancer immunotherapy. The characteristics of FA-PTX NAs were studied, and the cytotoxicity, cellular uptake, and DC stimulation of FA-PTX NAs were evaluated *in vitro* using a Lewis lung carcinoma (LLC) cell line and bone marrow-derived cells (BMDCs). Following this, the effect of the reprogrammed TIME and on the sensitization to immunotherapy *in vivo* were examined in a C57BL/6 mouse LLC subcutaneous xenograft model.

Results: The prepared FA-PTX NAs exhibited a slightly negative surface charge, appropriate size and shape, good drug release profiles, and high drug encapsulation efficiency and blood compatibility. The FA-PTX NAs were effectively uptaken by bone BMDCs, increasing the activation and expression of the costimulatory factor of BMDCs *in vitro*. In the LLC xenograft model treated with intravenous injection of FA-PTX NAs, the numbers of $CD4^+$ and $CD8^+$ T cells in the TIME increased significantly, the killing activity of tumor-specific cytotoxic T lymphocytes (CTLs) was significantly enhanced, and at the same time, the concentration of transforming growth factor β (TGF-β) decreased significantly. Furthermore, the infiltrated $CD8^+$ T cells in TIME were mainly distributed in the tumor parenchyma. The combination of FA-PTX NAs and ICIs effectively inhibited the growth of LLC xenograft tumor, demonstrating a greater effect than that of ICIs alone. Moreover, it was found that apoptosis induction, increase in $CD4^+$ and $CD8^+$ T-cell infiltration, and improvement in the distribution of $CD8^+$ T cells were involved in the anticancer mechanism of this combination treatment.

Conclusions: The NA loaded with low-dose PTX can reprogram the DC function in the TIME and exert

^ ORCID: 0000-0002-2718-0860.

a synergistic anticancer effect with ICIs in lung cancer treatment. Increased sensitization to ICI therapy as stimulated by PTX-enhanced NAs has potential applications in lung cancer immunotherapy.

Keywords: Lung cancer; immunotherapy; paclitaxel (PTX); nanoassemblies (NAs); tumor immune microenvironment (TIME)

Submitted Feb 19, 2025. Accepted for publication Apr 08, 2025. Published online Apr 23, 2025.
doi: 10.21037/tlcr-2025-180
View this article at: https://dx.doi.org/10.21037/tlcr-2025-180

Introduction

Lung cancer is the leading cause of cancer-related death worldwide (1). Cancer immunotherapy harnesses the host's own immune system to fight cancer and has robust and durable tumor remission effects. Therapeutic antibodies against the programmed cell death protein-1/programmed death-ligand 1 (PD-1/PD-L1) pathway have been approved in use alone or in combination with chemotherapy for first-line treatment in patients with non-small cell lung cancer (NSCLC) without alteration of driver genes. However, only approximately 20–40% of patients with NSCLC respond to immune checkpoint inhibitor (ICI) treatment (2-5). Therefore, novel therapeutic strategies for lung cancer immunotherapy are urgently required.

Immune tolerance of the tumor immune microenvironment (TIME) remains the most significant challenge in cancer immunotherapy. The specific antitumor immunotherapy response relies on the number, function, and distribution of infiltrating lymphocytes in the tumor microenvironment (6-8). As important antigen-presenting cells (APCs), dendritic cells (DCs) play a pivotal role in initiating this specific antitumor immunity. The maturation and activation of DCs can trigger an adaptive antitumor immune response (9,10). However, the immunosuppressive tumor microenvironment suppresses the activation and maturation of DCs.

Paclitaxel (PTX), a microtubule-disrupting chemotherapeutic drug, has been used to treat various cancers, including lung cancer, by inhibiting the proliferation of cancer cells. However, the traditional dosage of PTX used in clinic could lead to the death of immunogenic tumor cells while also causing apoptosis of immune cells due to the lack of specific targeting ability, which greatly affects the efficacy of cancer immunotherapy (11). Some recent studies have shown that a low-dose of PTX, as an immunomodulator, can enhance anticancer effects by stimulating the immune system without exerting obvious cytotoxicity to immune cells (12,13). Zhong *et al.* found that the application of noncytotoxic low-dose PTX promoted the maturation and activation of DCs *in vitro*. Meanwhile, it significantly reduced the inhibition of DC maturational ability caused by tumor cells (13). Therefore, targeting the activation of DCs

Highlight box

Key findings

- Nanoassemblies (NAs) targeting folate receptors can effectively deliver drugs to the tumor microenvironment.
- NAs loaded with low-dose paclitaxel (PTX) can reprogram the immunosuppressive tumor microenvironment by activating dendritic cells.
- NAs loaded with low-dose PTX can enhance the antitumor effect of immune checkpoint inhibitors (ICIs) in the treatment of lung cancer.

What is known and what is new?

- The therapeutic efficacy of ICIs is closely related to the immune status of the tumor microenvironment. Reprogramming the immunosuppressive tumor microenvironment can enhance the efficacy of ICI therapy.
- A drug-delivery system using a lipophilic lipid prodrug targeting folate receptors delivers drugs to the tumor microenvironment. NAs loaded with low-dose PTX enhance the efficacy of ICIs by reprogramming the immunosuppressive tumor microenvironment.

What is the implication, and what should change now?

- Our study indicates that combining PTX-enhanced nanoparticles with ICI treatment could be a viable, novel strategy for cancer immunotherapy, providing a synergistic antitumor effect but no significant cytotoxicity. This strategy has also prompted the design of a combined therapy of chemotherapeutic drugs and immunotherapy.

in the tumor microenvironment may be a feasible approach to improving the efficacy of immunotherapy.

Nanotechnology provides a platform for potent payloads to act on target cells and anatomical locations and has been used for the development and delivery of therapeutics (14,15). In recent years, it has been found that highly hydrophobic lipophilic prodrugs (LPs), obtained by combining hydrophobic drugs with hydrophobic elements (e.g., fatty acids and squalene), can be dispersed in water and self-assembled into stable nanoassemblies (NAs) without the aid of surface stabilizers (16,17). More importantly, functionalized components can be modularly embedded in LP-NAs to improve their tumor-targeting efficacy (18,19). The LP strategy has been used to deliver a variety of chemotherapeutics (e.g., PTX and docetaxel) with the advantage of high drug-loading capability (20-22). In addition, apart from being used for drug delivery, the multifunctional platform based on various nano-carriers can also be applied to cancer treatment (23). For example, the glycation reaction, especially the accumulation of advanced glycation end products (AGEs), is an important factor contributing to the occurrence and development of cancer. The synthesis of titanium dioxide (TiO_2) nanoparticles using the methanolic extract of medicinal plants and multimodal NAs have demonstrated good antiglycation and anticancer effects (24,25).

Inspired by the findings mentioned above, we designed a conjugate of lipophilic oleyl alcohol (OA) and PTX to form the lipophilic prodrug OA-PTX. OA-PTX and dis tearoylphosphatidylethanolamine-methoxy polyethylene glycol 2000-folic acid (DSPE-mPEG2000-FA) self-assemble to form folic acid-modified NAs, namely FA-PTX NAs. Incorporating DSPE-mPEG2000 during the self-assembly process further improves the colloidal stability of the prepared FA-PTX NAs. The FA-PTX NAs obtained exhibited a slightly negative surface charge, appropriate size and shape, good drug release profiles, and high drug encapsulation efficiency. Folic acid-modified NAs loaded with low-dose PTX can effectively reprogram the immunosuppressive tumor microenvironment and significantly enhance the efficacy of ICIs in the treatment of Lewis lung carcinoma (LLC). We present this article in accordance with the ARRIVE and MDAR reporting checklists (available at https://tlcr.amegroups.com/article/view/10.21037/tlcr-2025-180/rc).

Methods

Materials

PTX was purchased from Meilun Biology Technology Co., Ltd. (Dalian, China); DSPE-PEG2000 was purchased from Lipoid GmbH (Ludwigshafen, Germany); DSPE-PEG2000-FA was purchased from AVT Pharmaceutical Tech Co., Ltd (Shanghai, China); 3-(4,5-dimethylthiazol-2-yl)-2,5-diphenyl tetrazolium bromide (MTT) and coumarin-6 were purchased from Sigma-Aldrich (St. Louis, MI, USA); and Dulbecco's Modified Eagle's Medium (DMEM), fetal bovine serum (FBS), penicillin, and streptomycin were purchased from HyClone (GE Healthcare, Chicago, IL, USA). All solvents used in this study were of analytical grade.

Cell line and culture

The LLC cell line was purchased from the American Type Culture Collection (ATCC; Manassas, VI, USA) and cultured in DMEM medium supplemented with 10% FBS, 2 mM of L-glutamine, 100 U/mL of penicillin, and 100 μg/mL of streptomycin in a humidified chamber containing 5% CO_2 at 37 ℃.

Animals

Female C57BL/6 mice (4–6 weeks old) and male Sprague-Dawley (SD) rats (5–7 weeks old) were purchased from Beijing HFK Bioscience Co. Ltd (Beijing, China). Animals were housed under specific pathogen-free conditions with food and water in a laboratory animal room for animal experiments. All animals were cared for in accordance with the guidelines outlined in the *Guide for the Care and Use of Laboratory Animals*, *8th edition*. The animal experiments were approved and supervised by the Institutional Animal Care and Treatment Committee of the Chongqing University Cancer Hospital. A protocol was prepared before the study without registration.

Synthesis of OA-ACSS-PTX

Dithiodiglycolic acid (1 g) was dissolved in 40 mL of dichloromethane (DCM). 1,3-Dicyclohexylcarbodiimide (DCC) (1.0 equivalent), oleyl alcohol (OA) (1.0 equivalent),

and 4-Dimethylaminopyridine (DMAP) (~25 mg) were added and stirred at room temperature overnight. After the DCM was removed, 50 mL of ethyl acetate (EA) was added, and the solution was filtered to remove Dicyclohexylurea (DCU). The filtrate was further purified by silica gel column chromatography (200 mL petroleum ether (PE), 100 mL of PE–EA at 5:1, 100 mL of PE–EA at 4:1, and 200 mL of PE/EA at 2:1) to produce OA-ACSS-COOH.

To synthesize OA-ACSS-PTX, the OA-ACSS-COOH. (200 mg) was dissolved in anhydrous DCM (20 mL). DCC (1.2 eq), PTX (1.0 eq), and DMAP (~1 mg) were added and stirred at room temperature overnight. After DCM was removed, EA was added, and the solution was filtered to remove DCU. The filtrate was purified by silica gel column chromatography (400 mL PE–EA at 20:1) to obtain the OA-ACSS-PTX.

Preparation and characterization of PTX-loaded DSPE-mPEG2000-FA NAs

The FA-PTX NAs were prepared via the nanoprecipitation method. Briefly, a predetermined amount of OA-PTX, 10 mg of DSPE-mPEG2000 (10 wt%), and 1 mg of DSPE-mPEG2000-FA (1 wt%) were co-dissolved in ethanol to obtain a clear solution, which was then added dropwise to distilled water under vigorous stirring. The FA-PTX NAs were then evaporated under vacuum at 50 ℃ to the desired concentration. Fluorescence-labeled FA-PTX NAs were prepared by additionally incorporating 0.1 mg of coumarin-6. FA NAs were produced in a similar manner, free of encapsulation of OA-PTX.

The particle size and zeta potential of the FA-PTX NAs were measured by dynamic light scattering (DLS) via a Zetasizer Nano ZS (Malvern Instruments Ltd., Malvern, UK). The surface morphologies of the FA-PTX NAs were examined using a transmission electron microscope (TEM) (H-6009IV; Hitachi Ltd., Tokyo, Japan).

Hemolytic and aggregation assay of erythrocytes in vitro

Briefly, fresh blood from Sprague-Dawley rats was collected in heparinized tubes and washed with normal saline (NS) until the supernatant was colorless. Different concentrations (equivalent concentrations of PTX were 10, 20, 40, 80, and 160 μg/mL, respectively) of FA-PTX NAs in 0.5 mL of solution were added to 0.5 mL of rat erythrocyte suspension (4%) at 37 ℃. An erythrocyte suspension containing normal saline or distilled water was used as the negative or positive control, respectively. After 3 hours of incubation, all groups were centrifuged at 724 ×g for 3 minutes, and the supernatant was collected to determine the light absorbance value. The red supernatant solution indicated hemolysis, whereas the absolute achromatic supernatant solution indicated no hemolysis.

To detect erythrocyte aggregation, 100 μL of FA NAs or FA-PTX NAs (containing a PTX equivalent of 160 μg/mL) was coincubated with 100 μL of erythrocyte suspension (4%) in 12-well plates (Corning, Corning, NY, USA) at 37 ℃. After 2 hours of culture, erythrocyte aggregation was observed with an optical microscope (Olympus, Tokyo, Japan).

Encapsulation efficiency of FA-PTX NAs

To study the drug encapsulation efficiency of FA-PTX NAs, the concentrations of PTX were measured using high-performance liquid chromatography (HPLC) instrument (1100 HPLC, Agilent Technologies, Santa Clara, CA, USA). The mobile phase consisted of a mixture of acetonitrile and double-distilled water (60/40, v/v) pumped at a flow rate of 1.0 mL/min with a determination wavelength of 227 nm at 35 ℃. The following equation was used to calculate the drug encapsulation efficiency:

$$\text{Encapsulation efficiency} = \frac{\text{wt of the drug in nanoparticles}}{\text{wt of the feeding drug}} \times 100\% \quad [1]$$

Drug release assay in vitro

The amount of PTX released from FA-PTX NAs was measured using the dialysis method. FA-PTX NAs were diluted with phosphate-buffered saline (PBS) at a pH of 7.4 and 3.0. The solution was then sealed in a dialysis bag with a 3.5-kDa molecular weight cutoff [Sigma-Aldrich (Shanghai) Trading Co., Ltd.] and immersed in 10 mL of 0.1 mol/L PBS at a pH of 7.4 or 3.0, a temperature of 37 ℃, and at 2.2 ×g centrifugation. At each time point (0, 2, 5, 10, and 24 hours), 100 μL of the sample was collected from the incubation medium for HPLC. An equal volume of fresh PBS was added to the incubation medium immediately after sampling. The concentration of PTX released from FA-PTX NAs was calculated as a percentage of the total PTX in the FA-PTX NAs and plotted as a function of time.

Bone marrow-derived dendritic cell (BMDC) culture

BMDCs were derived from C57BL/6 mice in a manner described previously (26). Briefly, the tibia and femoral bone marrow cells were isolated and processed using red blood cell lysis buffer for 2 minutes. After two washes with RPMI-1640 medium, the cells were resuspended in RPMI-1640 medium containing Granulocyte-Macrophage Colony-Stimulating Factor (GM-CSF) and IL-4 at a final concentration of 10 ng/mL. After 48 hours of cultivation in an incubator at 37 ℃ in a 5% CO_2 atmosphere, all cells were centrifuged and resuspended in fresh medium. The medium was changed every 2 days. All suspended cells were collected on day 7, and rich BMDCs were obtained.

Cell viability and apoptosis detection

LLC cells and BMDCs were collected and replanted in a 96-well plate at a density of 5×10^3 cells per well and cultured for 24 hours. The cells were then treated with FA NAs, FA-PTX NAs, and PTX at different PTX equivalent concentrations. After incubation for another 24 hours, the MTT reagent was added and the absorbance value was measured with a multiwell spectrophotometer (BioTek Instruments, Winooski, VT, USA) at 570 nm. Cell viability was calculated as a percentage of untreated controls that were not exposed to drugs.

To evaluate apoptosis in LLC and BMDCs, the Annexin V binding assay was done. LLC and BMDCs cells were seeded in a 6-well plate at a density of 1.5×10^5 cells per well and the treatment procedures were the same as the mentioned above. 24 h after treatments, the rate of apoptosis was measured on the flow cytometry (Beckman-Coulter) using the Annexin V-FITC Apoptosis Detection Kit I (BD Biosciences, San Jose, CA), in accordance with the manufacture's protocol.

Cellular uptake and DC stimulation assay in vitro

FA-PTX NAs and PTX NAs were labeled with coumarin-6 to investigate their cellular uptake by BMDCs *in vitro*. Day 7 BMDCs were coincubated with coumarin-6-labeled FA-PTX NAs for 4 hours in a six-well plate. The cells were then washed with cold PBS after incubation and immobilized with paraformaldehyde (4%) for 30 minutes. Finally, the cellular uptake of FA-PTX NAs or PTX NAs *in vitro* was qualitatively measured under a confocal scanning laser microscope (Olympus) and quantified with a flow cytometer (Beckman Coulter, Brea, CA, USA).

Day 7 BMDCs were used to investigate the stimulation effect of FA-PTX NAs in DCs. BMDCs treated with FA-PTX NAs were coincubated with LLC cells for 48 hours, and the cells were collected and costained with anti-CD80 (APCs), anti-CD86 (PE), and anti-CD11c [fluorescein isothiocyanate (FITC)] antibodies. Flow cytometry was used to analyze the abundance of CD80+CD86+CD11c+ BMDCs.

Western blot analysis

The total protein concentrations of cell lysates from BMDCs treated with FA-PTX NAs were quantified by using the BCA Protein Assay Kit (Beyotime, China). Proteins from each sample were loaded into 12% sodium dodecyl sulfate-polyacrylamide gel electrophoresis and transferred to poly(vinylidene difluoride) membranes (Millipore). The membranes were sealed by using 5% skimmed milk, then incubated with anti-β-actin (Santa Cruz Biotechnology Inc.) or anti-MyD88 primary antibody (Proteintech, china) separately overnight at 4 ℃. The membranes were further incubated with relevant secondary antibody, which is labeled with horseradish peroxidase and colorated by the enhanced chemiluminescence detection reagents (EMD Millipore).

Establishment of LLC xenograft model

Female C57BL/6 mice were inoculated by subcutaneous injection into their backs with 200 μL of LLC cell suspension (5×10^6 cells). When the tumor volume reached approximately 100 mm^3 in volume, subsequent experiments were performed.

Tumor-targeting assay and biodistribution

LLC tumor-bearing mice were used to perform a targeting tumor ability assay and biodistribution for FA-PTX NAs *in vivo*. Coumarin-labeled FA-PTX NAs were injected intravenously into the tail vein. At different time points (0, 8, 12, 16, 20 and 24 hours) after administration, a live image analysis instrument (Caliper Life Sciences, Hopkinton, MA,

USA) was used for fluorescence imaging to determine the drug biodistribution.

Flow cytometry

To evaluate the ability of PTX to improve the immune state in the TIME, LLC tumor-bearing mice were treated with NS and FA NAs containing different PTX equivalent doses via intravenous injection. The LLC tumors taken from C57BL/6 mice were washed with ice-cold PBS (pH 7.4) to remove any remaining blood and then dissociated via the mincing of tissue with scalpels, which was followed by the addition of DMEM containing 1 mg/mL of collagenase I and incubation for 60–90 minutes at 37 ℃. The dissociated tumor tissue was washed with ice-cold PBS and filtered through a 70-μm cell strainer (BD Biosciences, Franklin Lakes, NJ, USA). The cell suspension was then centrifuged at a speed of 224 ×g for 5 minutes at 4 ℃. The cells were resuspended in 100 μL of PBS for further analysis. The cell suspensions were then stained with fluorochrome-labeled antibody-targeting murine CD4-FITC (eBioscience, San Diego, CA, USA), CD8-APC (Life Technologies, Thermo Fisher Scientific, Waltham, MA, USA), or an appropriate isotype control antibody and then analyzed by flow cytometry (Beckman Coulter, Brea, CA, USA). The results were analyzed using Kaluza Analysis Software version 1.3 (Beckman Coulter).

Enzyme-linked immunosorbent assay

LLC tumors collected from C57BL/6 mice were ground into powder with liquid nitrogen in grinding bowls and then homogenized in radioimmunoprecipitation assay (RIPA) lysis buffer (Beyotime Bioscience, Nantong, China), followed by centrifugation at 19776 ×g for 30 minutes at 4 ℃. The 4-Diethylaminobenzaldehyde (DEAB) assay was used to test the protein concentration of samples. The prepared samples were stored at –80 ℃ until used. The levels of TGF-β in the samples were measured using mouse enzyme-linked immunosorbent assay (ELISA) kits (eBioscience) according to the manufacturer's instructions, and the colorimetric reaction was measured at 450 nm using a microplate reader (Benchmark Electronics, Angleton, TX, USA).

Immunohistochemical analysis

LLC tumors from C57BL/6 mice were immediately fixed in formalin and embedded in paraffin. Paraffin (thickness 5 μm) sections were used to detect the presence of $CD4^+$ and $CD8^+$ T cells. Sections were incubated at 4 ℃ overnight with anti-mouse CD4 or anti-mouse CD8 antibodies (Abcam, Cambridge, UK), followed by incubation with appropriate secondary antibodies (Abcam). Peroxidase activity was visualized using a 3,3'-diaminobenzidine (DAB) substrate kit (Beyotime Bioscience, China). The sections were counterstained with hematoxylin. The slides were examined under a microscope (Eclipse E600; Nikon, Tokyo, Japan).

Isolation of splenic T cells and cytotoxicity assay

To detect splenic T cell activity, single-cell suspensions were obtained by lysis of erythrocytes using M-Lyse buffer (R&D, Minneapolis, MN, USA). Cytotoxicity against target cells was analyzed using the CytoTox 96 Non-Radioactive Cytotoxicity Assay-Lactate Dehydrogenase release assay (Promega, Madison, WI, USA), according to the manufacturer's instructions. Briefly, splenic T cells were seeded in two 96-well plates at 1×10^5 cells/well and incubated for 48 hours with cells at a 20:1 effector-to-target (E-to-T) ratio. A volume of 30 μL of cell culture supernatant was transferred to transparent flat-bottom 96-well plates, and then 30 μL of substrate was added. After incubation for 30 minutes in the dark at room temperature, the reaction was stopped by adding 30 μL of stop solution. Thereafter, the absorbance was measured at 490 nm. The maximal release of lactate dehydrogenase was achieved by complete lysis of the target cells. Target or effector cells alone were used as negative controls (spontaneous release). The killing rate was determined using the following formula:

$$\text{Killing rate} = \frac{\text{experimental counts} - \text{effector control counts} - \text{target spontaneous counts}}{\text{target maximal counts} - \text{target spontaneous counts}} \times 100\% \quad [2]$$

Antitumor efficacy in vivo

LLC tumor-bearing mice were randomly assigned to six groups (n=5) and treated with NS, FA NAs, FA-PTX NAs, NS + anti-PD-1, FA NAs + anti-PD-1, or FA-PTX NAs + anti-PD-1 via intravenous injection. Tumor volume and body weight were recorded every 3 days from the first dose of administration. Tumor volumes were calculated as follows: tumor volume = 0.5 × length × width^2. Mice were killed via cervical vertebra dislocation 21 days after the first dose of administration, and the heart, liver, spleen, lung, kidney, and tumors were collected for hematoxylin and eosin (HE) staining, immunohistochemical (IHC) analysis, and ELISA. Tumor weights of the mice were recorded. Moreover, survival times were recorded every 3 days until 35 days after the first dose of administration.

Histological analysis and HE staining

The tissues were fixed in neutral paraformaldehyde (4%) for at least 24 hours and then embedded in paraffin. A commercially available terminal deoxynucleotidyl transferase 2'-deoxyuridine 5'-triphosphate nick end labeling (TUNEL) kit (Promega, Madison, WI, USA) was used to detect apoptotic cells in the tumor tissues in paraffin sections according to the manufacturer's instructions. HE staining of the sections was performed to analyze the histomorphometry of tumor tissues.

Safety evaluation

Vital organs (liver, heart, lung, spleen, and kidney) and serum were harvested. HE staining and ELISA assay using standard methods to evaluate the potential toxicity of the FA-PTX NAs and anti-PD-1 combined treatment.

Statistical analysis

All data are presented as the mean ± standard deviation. All experiments were repeated at least three times. For a single comparison of two groups, the Student's *t*-test is used after evaluating the normality of the data. If the data distribution is not normal, a Mann-Whitney rank sum test is conducted. For the comparison of multiple groups of data, one-way or two-way analysis of variance (ANOVA) is applied. Differences were considered statistically significant at P<0.05. The survival rates of mice were generated based on the Kaplan-Meier method, and statistical significance was determined via the log-rank test. A P value <0.05 was considered statistically significant.

Results

Preparation and characterization of FA-PTX NAs

First of all, we designed a highly lipophilic prodrug delivery platform to deliver the hydrophobic drug PTX to the tumor microenvironment. To resist the acidic environments in the tumor microenvironment and within cells, we chose OA, an acid-stable lipid, as the carrier. PTX was conjugated with OA via the disulfanyl acetate (ACSS) linker to be modified into the corresponding lipophilic prodrug, OA-ACSS-PTX (*Figure 1A*). Subsequently, the prepared OA-PTX and DSPE-mPEG2000-FA could readily assemble into FA-PTX NAs in water with a semitransparent appearance. During this process, DSPE-mPEG2000 was added to enhance the targeting ability and spatial stability of the NAs (*Figure 1B*). DLS measurements showed that the mean particle size of the FA-PTX NAs was 117±8 nm [Polydispersity Index (PDI) =0.18], which was slightly larger than that of the FA NAs (110±6 nm) (PDI =0.14) (*Figure 2A*), and no statistical difference was found (P>0.05). As shown in *Figure 2B*, the mean zeta potential of FA-PTX NAs was –23.2±1.9 mV, showing no significant difference from that of FA NAs at –22.9±2.3 mV. TEM analysis revealed that the FA-PTX NAs had a sphere-like morphology with a mean particle diameter of approximately 90 nm, which was similar to that of FA NAs (*Figure 2C*).

To study the encapsulation ability of PTX based on FA NAs, we mixed PTX and FA NAs (the sum of DSPE-mPEG2000 and DSPE-mPEG2000-FA) in different ratios (1:10, 1:50, and 1:100 w/w). The results indicated that the encapsulation efficiency of PTX was over 90% even when the ratio of PTX to FA-NAs was 1:10, as shown in *Figure 2D*.

To simulate the release behavior of FA-PTX NAs in blood and inside cells *in vitro*, we incubated FA-PTX NAs in PBS at 37 ℃ and pH 7.4 and pH 3.0. The release profiles (*Figure 2E*) indicated that PTX was released slowly from the FA-PTX NAs at both a pH of 7.4 and pH 3.0. The release was even slower in an acidic environment. Within 48 hours, the cumulative release of PTX in the pH 7.4 and pH 3.0 environments only reached 53.1% and 36.4%, respectively.

Moreover, we carried out erythrocyte aggregation and hemolysis assay to evaluate the blood compatibility of FA-PTX NAs. As shown in *Figure 2F,2G*, the FA-PTX NAs caused no obvious hemolysis or hemagglutination at the

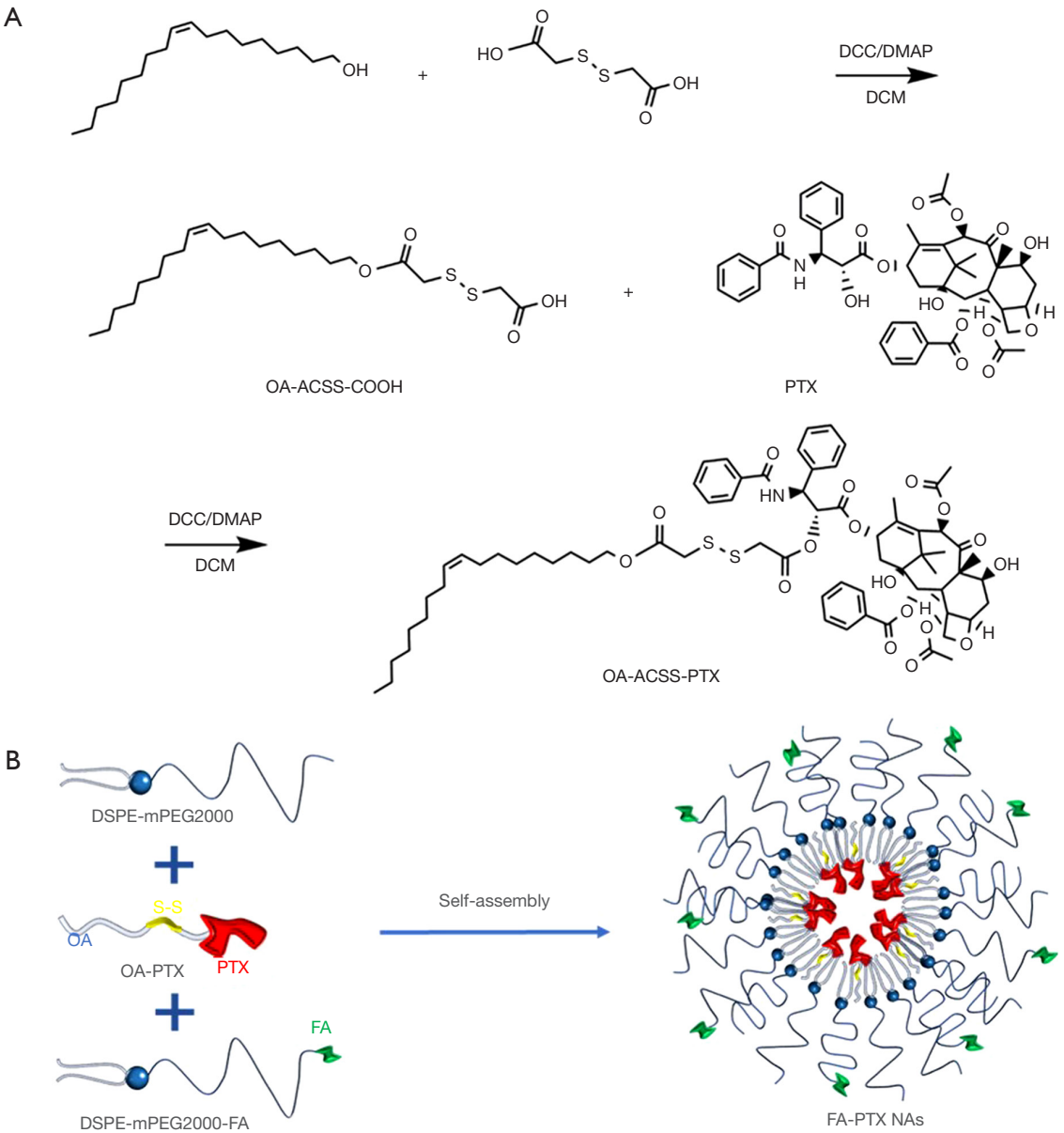

Figure 1 Preparation of FA-PTX NAs. (A) Synthesis route of OA-PTX. (B) Diagram of FA-PTX NA preparation. DCC, dicyclohexylcarbodiimide; DCM, dichloromethane; DMAP, 4-dimethylaminopyridine; FA-PTX NA, folic acid-modified nanoassemblies loaded with paclitaxel; OA-PTX, oleyl alcohol paclitaxel.

experimental concentration, which suggested that the FA-PTX NAs had good blood compatibility and were suitable for intravenous medication.

Cell viability and cellular uptake in vitro

The MTT assay was used to detect the cytotoxicity of FA-PTX NAs and FA NAs in BMDCs or LLC cells *in vitro*. As shown in *Figure 3A*,*3B*, the cytotoxicity of FA-PTX NAs and PTX on BMDCs or LLC cells was dose-dependent. When the equivalent concentration of PTX or FA-PTX NAs was lower than 5 μg/mL, neither PTX nor FA-PTX NAs showed cytotoxicity to BMDCs or LLC cells. When the equivalent concentration of PTX was higher than 20 μg/mL, PTX exhibited increased cytotoxicity. However, FA-PTX NAs showed only approximately 30%

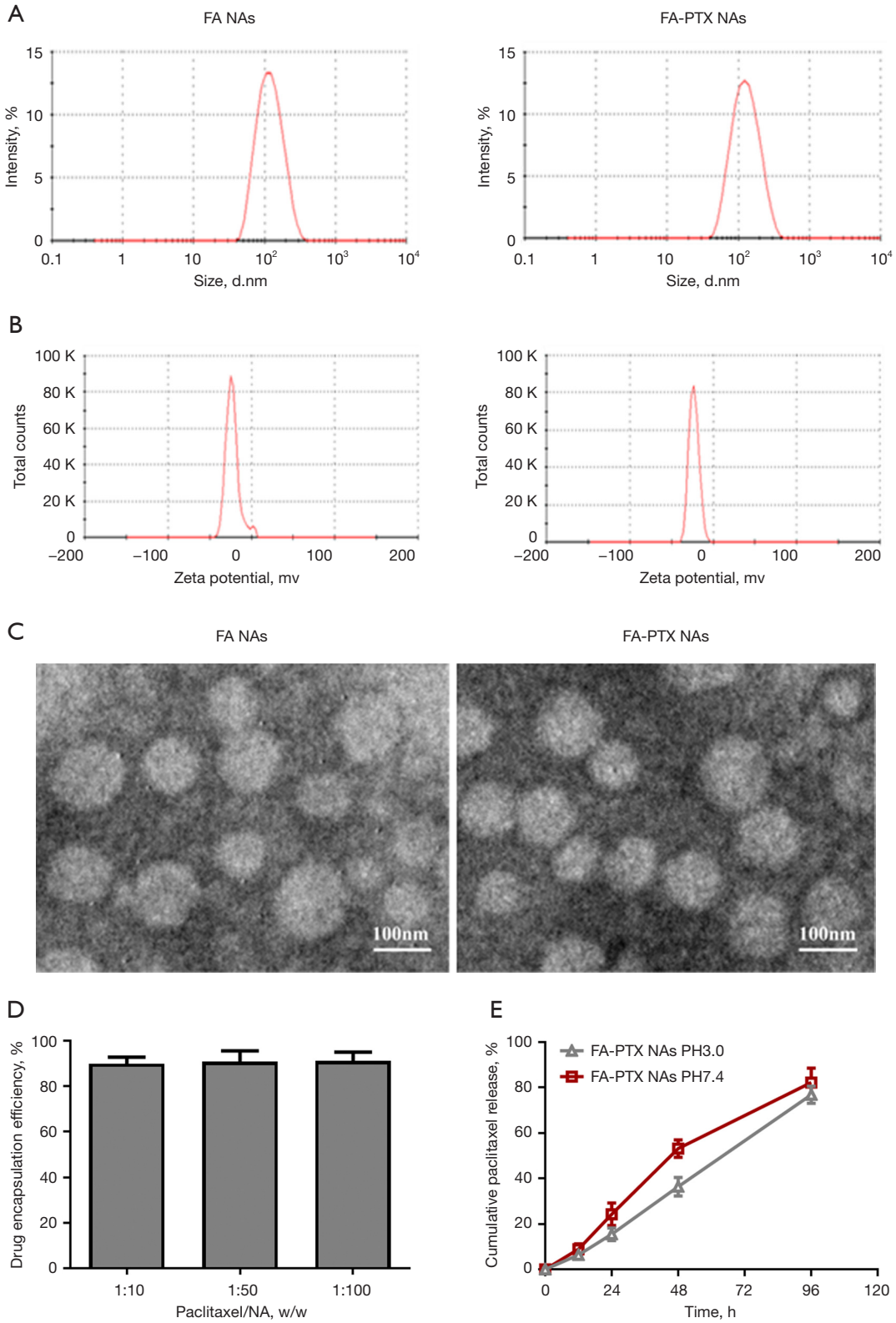

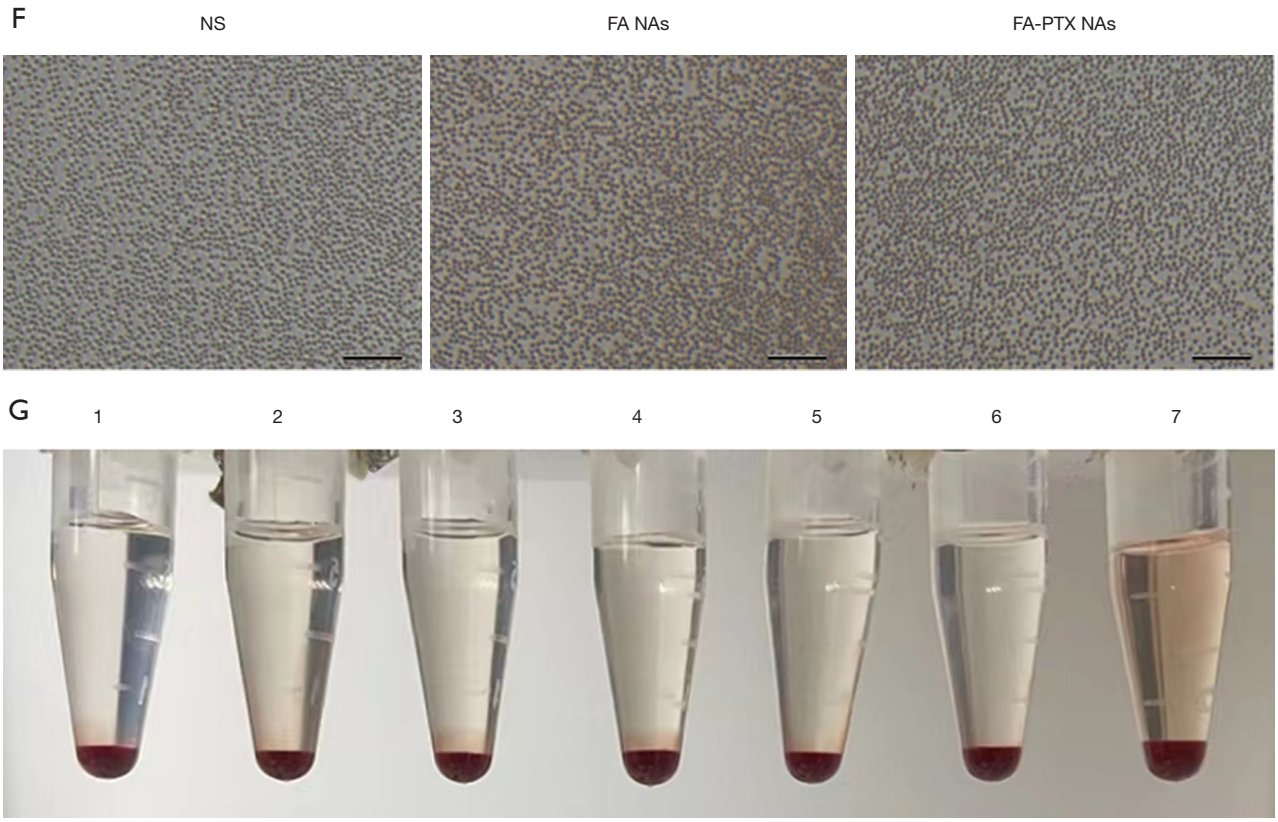

Figure 2 Characterization of FA-PTX NAs. (A) Size distribution spectrum and (B) zeta potential spectrum determined by Zetasizer Nano ZS. (C) Morphologic feature determined by a transmission electron microscopic image. Scale bar =100 nm. (D) Encapsulation efficiency and (E) release profile of paclitaxel determined by HPLC. (F) Erythrocyte aggregation assay observed with an optical microscope. Scale bar =100 μm. (G) Hemolytic test: PTX equivalent concentrations of [1] 10 μg/mL, [2] 20 μg/mL, [3] 40 μg/mL, [4] 80 μg/mL, and [5] 160 μg/mL, along with [6] normal saline (negative control) and [7] distilled water (positive control). FA NAs, folic acid-modified nanoassemblies; FA-PTX NA, folic acid-modified nanoassemblies loaded with paclitaxel; HPLC, high-performance liquid chromatography; NS, normal saline.

growth inhibition of BMDCs or LLC cells even when the concentration reached 100 μg/mL. Compared with free PTX, FA-PTX NAs showed lower cytotoxicity to LLC and BMDCs, which might have been due to the slow and sustained release of PTX from FA-PTX NAs. In addition, we also investigated the cytotoxicity of FA NAs to LLC and BMDCs. As shown in *Figure 3C*, FA NAs had slight toxicity to LLC and BMDCs. Even when the concentration of FA NAs reached 200 μg/mL, the cell inhibition rates of the two groups of cells were only around 15%.

Furthermore, LLC and BMDCs cells were treated with a range of equivalent concentrations of PTX or FA NAs. The cells were harvested 24 hours later, and the sensitivities of LLC and BMDCs cells to various concentrations of PTX and FA NAs were further evaluated by assessing the level of cellular apoptosis. To represent the results related to the apoptosis rates of drug-treated LLC and BMDCs cells, we subtracted the percentage of spontaneous apoptotic in the untreated cell cultures from the drug-induced apoptosis values. The Annexin V binding assay showed that the apoptosis rate exhibited a dose-dependent pattern with respect to the PTX concentration. When the PTX concentration was 5 μg/mL, the apoptosis rates of the FA-PTX NAs group and the PTX group for LLC cells were 2.18% and 5.68% respectively, and for BMDCs cells were 2.46% and 2.09% respectively. When the PTX concentration was greater than 10 μg/mL, the apoptosis rates of the FA-PTX NAs group and the PTX group for both LLC and BMDCs cells increased significantly (*Figure 3D*,*3E*). We also evaluated the apoptosis rates of LLC and BMDCs cells induced by FA NAs. The results showed that even when the concentration of FA NAs

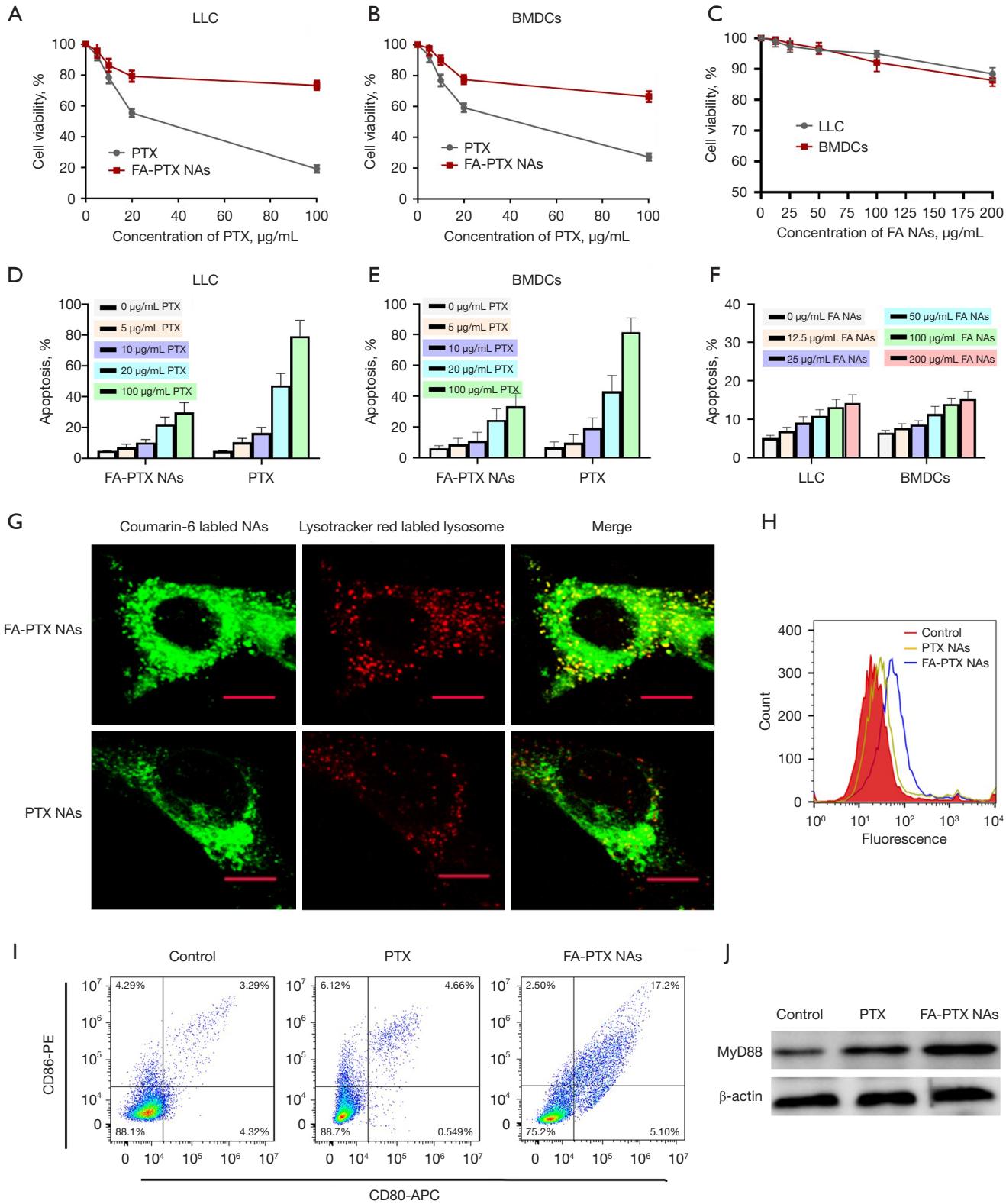

Figure 3 Cell viability, cellular uptake of FA-PTX NAs, and BMDC stimulation experiments. LLC and BMDCs cells incubated with FA-PTX NAs, PTX or FA NAs at indicated concentrations for 24 hours. Cell viability was detected by MTT assay (A-C) and cell apoptosis was

examined by flow cytometry (D-F). (G) Image from confocal laser scanning microscopy of cellular uptake and the (H) fluorescence peak of cells on the flow cytometry histogram. BMDCs treated with FA-PTX NAs (the equivalent PTX dose of 5 ng/mL) for 4 h. FA-PTX NAs were labeled with coumarin-6. Scale bar =10 μm. (I) Antigen expression of DCs after treatment with FA-PTX NAs and PTX (the proportion of $CD80^+CD86^+CD11c^+$ DCs was detected). (J) The expression of MyD88 was examined by western blot assay. BMDCs, bone marrow-derived cells; DCs, dendritic cells; FA-PTX NAs, folic acid-modified nanoassemblies loaded with paclitaxel; FA NA, folic acid-modified nanoassemblies; LLC, Lewis lung carcinoma; MTT, 3-(4,5-dimethylthiazol-2-yl)-2,5-diphenyl tetrazolium bromide; PTX, paclitaxel.

reached 200 μg/mL, the apoptosis rates of LLC and BMDCs cells induced by FA NAs were only 9.20% and 8.85% respectively (*Figure 3F*). This indicates that the prepared FA NAs are safe. Therefore, we chose a PTX equivalent concentration of 5 μg/mL for the subsequent BMDCs stimulation experiments.

DCs can engulf nanoparticles effectively, resulting in the clearance of nanoparticles. However, the phagocytosis of DCs provides an opportunity to deliver immunomodulators to promote DC maturation and initiate an adaptive immune response. Activated macrophages, which are important DCs, express folate receptor (27), and the expression of folate receptors further promotes phagocytosis of DCs. Therefore, we compared the cellular uptake of FA-PTX NAs and PTX NAs by BMDCs using confocal microscopy. Flow cytometry was used to compare the fluorescence intensity of the cellular uptake of FA-PTX NAs and PTX NAs. Under confocal laser scanning microscopy, the colocalization (yellow/orange) of coumarin - 6/FA-PTX NAs (green) and the lysotracker (red) within the same cells was clearly observed. This finding demonstrates that both FA-PTX NAs and PTX NAs are capable of being internalized by BMDCs. In comparison with coumarin-6/PTX NAs, coumarin-6/FA-PTX NAs led to a remarkable enhancement in cellular uptake (*Figure 3G*). The fluorescence intensity of cells incubated with FA-PTX NAs was much higher than that with PTX NAs (*Figure 3H*).

The phagocytosis and presentation of antigens by DCs play an important role in initiating the adaptive immune response. The expression of the costimulatory molecules CD40, CD80, and MHC II are all upregulated when immature DCs turn into mature DCs. To determine whether FA-PTX NAs could promote DC activation and maturation, we incubated BMDCs treated with free PTX or FA-PTX NAs. Subsequently, the expression of DC surface antigens was evaluated. The results indicated that the mean percentages of $CD11c^+CD80^+CD86^+$ treated with control, free PTX, and FA-PTX NAs were 3.29%±0.96%, 4.66%±1.20%, and 17.20%±3.15%, respectively (*Figure 3I*). Moreover, FA-PTX NAs were found to enhance the DC antigen presentation effect as compared to free PTX.

Next, we investigated the possible mechanism by which PTX enhances the maturation of BMDCs. Studies have shown that PTX can mimic bacterial lipopolysaccharide (LPS) and directly bind to Toll-like receptor 4 (TLR4), enhancing the maturation of DCs through the TLR4/MyD88/NF-κB signaling pathway. In the TLR4/MyD88/NF-κB signaling pathway, the activation of MyD88 plays a crucial role in promoting the nuclear translocation of downstream NF-κB and inducing the maturation of DCs (28,29). Therefore, we detected the expression of MyD88 protein by Western blot. The result showed that the expression level of MyD88 in BMDCs treated with FA-PTX NAs was significantly higher than that in cells treated with free PTX (*Figure 3J*).

Tumor-targeting assay in vivo

To evaluate the tumor-targeting ability of FA-PTX NAs *in vivo*, we intravenously injected coumarin-6-labeled FA-PTX NAs into tumor-bearing mice and observed the fluorescence intensity of the tumors at different time points. The real-time distribution images of FA-PTX NAs *in vivo* demonstrated that the fluorescence derived from coumarin-6 was mainly observed in tumor nodules, reaching its peak at 12 hours after administration, and almost disappeared 18-24 hours after administration. In addition, the fluorescence derived from coumarin-6 could also be detected in the liver and kidneys, but the fluorescence intensity in these sites was much lower than that in the tumor nodules (*Figure 4*).

Detection the proportion of $CD4^+$ and $CD8^+$ T cells in the TIME

To determine whether PTX encapsulated in FA NAs could improve the immune state of the TIME, we constructed a subcutaneous LLC xenograft model in C57BL/6 mice. Tumor-bearing mice were injected with FA-PTX NAs loaded with different doses of PTX at different time points. Flow cytometry was used to detect the proportion of $CD4^+$

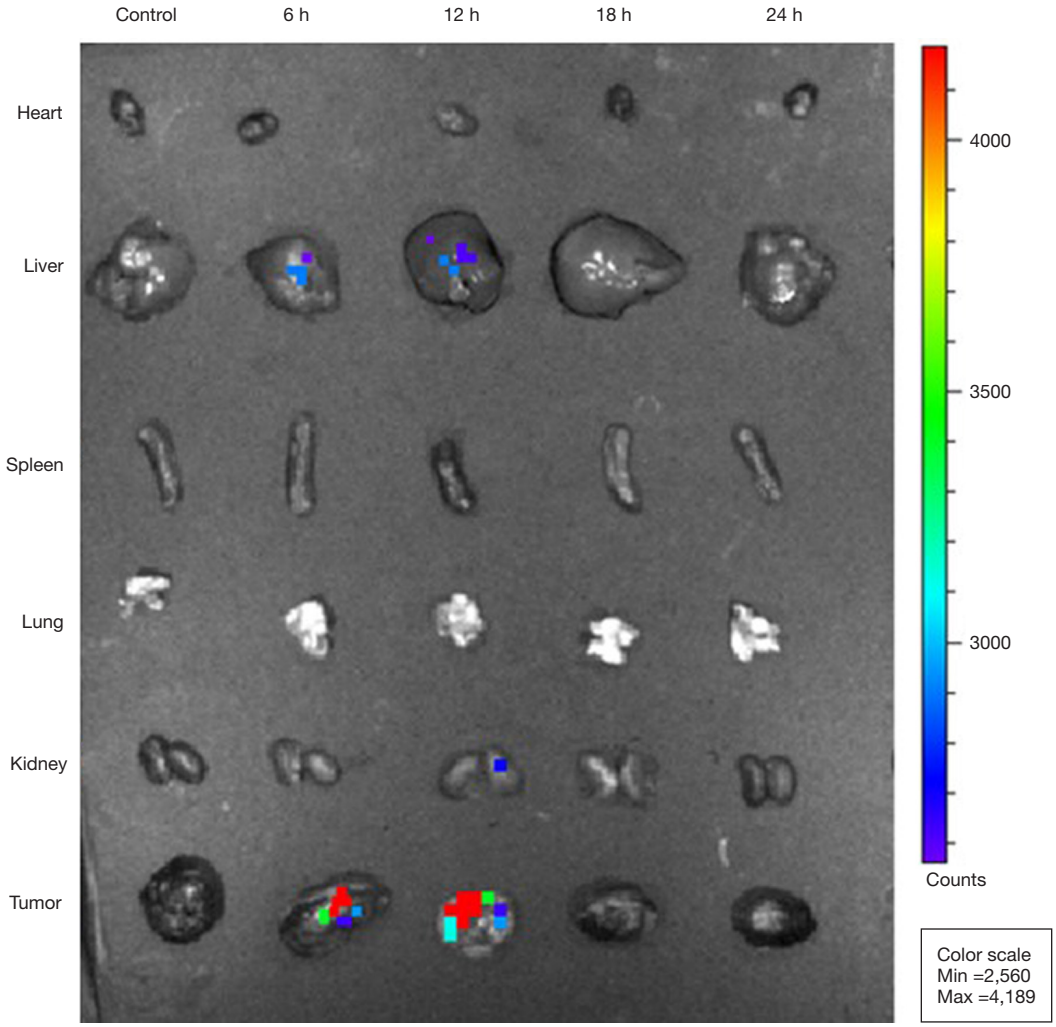

Figure 4 Tumor-targeting assay and biodistribution of FA-PTX NAs. Biodistribution image of FA-PTX NAs in tumor and vital organs (heart, liver, spleen, lung and kidney) at different time points after intravenous administration of the coumarin-6-labeled FA-PTX NAs as monitored by a live image analysis instrument. FA-PTX NAs, folic acid-modified nanoassemblies loaded with paclitaxel.

and $CD8^+$T cells at different time points, both of which corresponded to the anticancer response to ICIs. A schematic diagram of the injection procedure is shown in *Figure 5A*. Flow cytometry analysis showed that at 3, 5, or 8 days of administration, the proportion of the $CD4^+$ and $CD8^+$ T cells in the FA-PTX NA-treated groups were significantly higher than those in FA NA-treated groups and NS-treated groups; meanwhile, the proportion of $CD4^+$ and $CD8^+$ T cells in FA NA-treated groups were similar to those in the NS-treated groups. Moreover, the proportions of $CD4^+$ and $CD8^+$ T cells on day 3, 5, and 8 of administration increased as the equivalent dose of PTX increased from 0.1 to 1 mg/kg and then decreased when the equivalent dose of PTX exceeded 1 mg/kg, indicating that the dose of 1 mg/kg was the most appropriate dose. We compared the proportion of $CD4^+$ and $CD8^+$ T cells on days 3, 5, and 8 after administration and found that the proportions of $CD4^+$ and $CD8^+$ T cells on day 5 in each group were all higher than those on days 3 and 8; this indicated that 5 days after administration was the best time point for immune state improvement in the tumor microenvironment (*Figure 5B-5E*).

The abundance and distribution of $CD8^+$ T cells in the TIME

A study has shown that the response to ICIs is closely

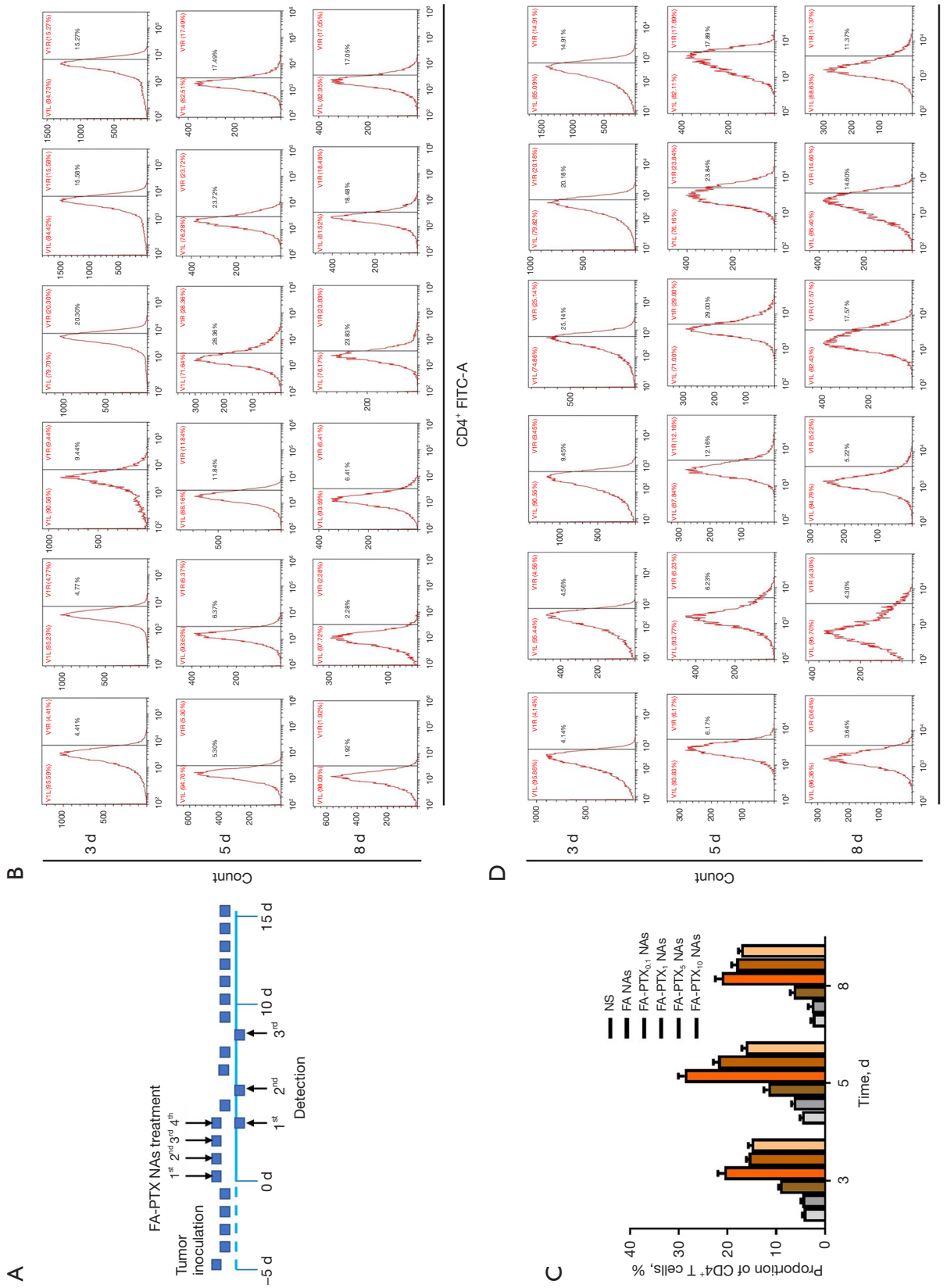
A
Tumor inoculation
FA-PTX NAs treatment
1st 2nd 3rd 4th
Detection
1st 2nd 3rd
−5 d
0 d
10 d
15 d
B
3 d
5 d
8 d
Count
CD4+ FITC-A
C
NS
FA NAs
FA-PTX0.1 NAs
FA-PTX1 NAs
FA-PTX5 NAs
FA-PTX10 NAs
Proportion of CD4+ T cells, %
Time, d
D
CD8+ APC-A

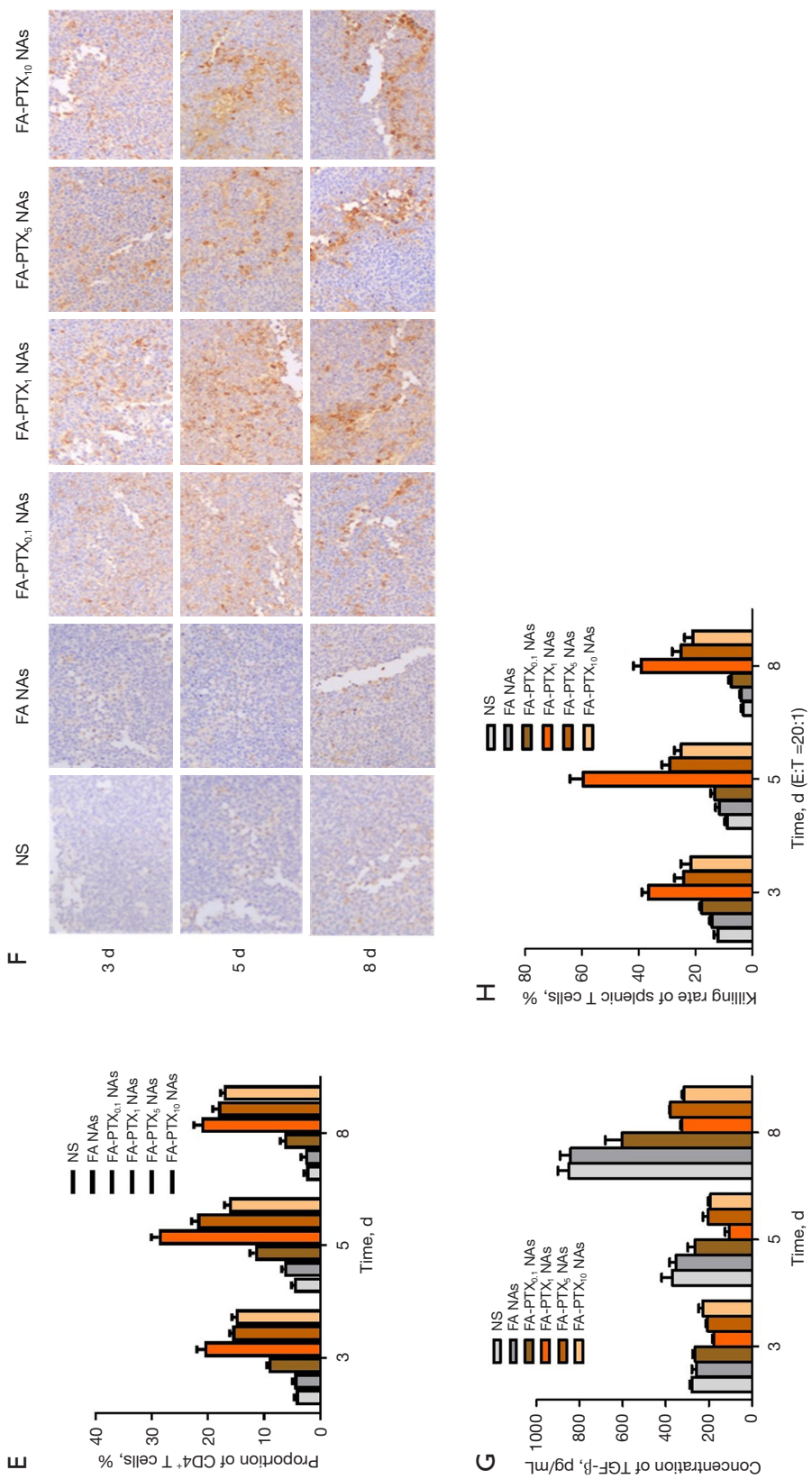

Figure 5 Detection of the immune state of the TIME. (A) Schematic diagram of the administration and detection schedule. The proportion of (B,C) $CD4^+$ T cells and (D,E) $CD8^+$ T cells of tumors from mice treated with NS, FA NAs, and FA-PTX NAs containing different doses of PTX at different time points as detected by flow cytometry. The numbers in the right area indicate the percentages of (B) $CD4^+$ or (D) $CD8^+$ T cells. (F) The distribution of $CD8^+$ T cells in the TIME as detected by IHC. Scale bar =100 μm. (G) The concentration of TGF-β detected in tumors via ELISA in the different treatment groups at different time points. (H) The killing rate of splenic T cells as measured by lactate dehydrogenase release assay. FA-PTX NA, folic acid-modified nanoassemblies loaded paclitaxel; FA NA, folic acid-modified nanoassemblies; IHC, immunohistochemical; NS, normal saline; TIME, tumor immune microenvironment; TGF-β, transforming growth factor-beta.

related to the distribution of $CD8^+$ T cells in the TIME and the number of $CD8^+$ T cells (30). We detected the abundance and distribution of the $CD8^+$ T cells in the TIME via IHC. The results revealed a low abundance of $CD8^+$ T and a sporadic distribution around vessels in the TIME among the groups treated with NS or FA NAs; meanwhile, in the FA-PTX NA treatment groups, a greater abundance of $CD8^+$ T cells was observed, and these cells were mainly located among tumor cells in the TIME on days 3, 5, and 8 of administration. In the FA-PTX NA groups, when the equivalent dose of PTX was 1 mg/kg, the greatest abundance of $CD8^+$ T cells were observed, and they were interspersed among the tumor cells. When the equivalent dose of PTX exceeded 1 mg/kg, the abundance of $CD8^+$ T cells remained unchanged, but there was a greater distribution of $CD8^+$ T cells around the blood vessels. Moreover, compared with that on days 3 and 8 of administration, the number of $CD8^+$ T cells in the TIME on day 5 of administration increased significantly and the distribution was more favorable (*Figure 5F*).

Concentration of TGF-β in the TIME

A study has revealed that TGF-β is closely associated with the infiltration and distribution of $CD8^+$ T cells in the TIME (30). We measured the concentration of TGF-β in the TIME using ELISA. The results showed that on day 3, 5, and 8 of administration, the amount of TGF-β in groups treated with FA-PTX NAs was significantly reduced compared with that in groups treated with NS or FA NAs, while the amount of TGF-β in the FA NA groups was slightly lower than that in the NS group. Moreover, the amount of TGF-β was the lowest in each FA-PTX NA treatment group on day 5 of administration than on days 3, 5, and 8 of administration and was the lowest in the FA-PTX_1 NA group among the different groups of equivalent PTX doses (*Figure 5G*).

Detection of tumor-specific cytotoxic T lymphocytes (CTLs)

The antitumor response of ICIs largely depends on the activity of tumor-specific CTLs. We performed a cytotoxicity assay to assess the cytotoxicity of splenic T cells against cancer cells using an *in vitro* lactate dehydrogenase release assay. After splenic T cells were cocultured with LLC cells for 48 hours at 20:1 E-to-T ratios, splenic T cells from mice treated with NS or FA NAs showed weak cytotoxicity for LLC cells, and the cytotoxicity decreased with time, with killing rates of 12.10%±1.24%, 14.12%±1.43% on day 3 of administration, 8.82%±0.78%, 11.50%±1.09% on day 5 of administration, and 3.14%±0.63%, 3.80%±0.78% on day 8 of administration. There were no differences in splenic T cell killing rates between mice treated with NS and FA-NAs. However, splenic T cells from mice treated with FA-PTX NAs showed stronger cytotoxicity in LLC cells than mice treated with NS or FA NAs. The killing rate of the FA-PTX_1 NAs groups was 36.63%±2.71% on day 3, 59.63%±4.18% on day 5, and 39.15%±4.74% on day 8. The killing rate of FA-PTX_1 NAs was also significantly higher than that of FA-$PTX_{0,1}$ NAs, FA-PTX_5 NAs, and FA-PTX_{10} NAs (*Figure 5H*).

Based on the above results, we chose the PTX equivalent dose of 1 mg/kg once a day 4 times on day 5 of administration for the injection of ICIs for subsequent experiments.

Antitumor efficacy in vivo

To improve the antitumor response to ICIs of FA-PTX NAs *in vivo*, we constructed a subcutaneous LLC xenograft tumor model in C57BL/6 mice and intravenously injected NS, FA NAs, FA-PTX NAs, and anti-PD-1 [an anti-mouse PD-1 (CD279)-in vivo, Bioxcell] (31). The FA-PTX NAs were administered once a day four times (the equivalent dose of PTX was 1 mg/kg) 5 days after tumor inoculation, and then anti-PD-1 was injected with 10 mg/kg every other day for a total of two doses on days 5 and 7 of administration. The treatment regimen is shown in *Figure 6A*. As shown in *Figure 6B*, NS + anti-PD-1, FA NAs + anti-PD-1, and FA-PTX NAs + anti-PD-1 all displayed significant tumor growth inhibition effects compared to NS, FA NAs, and FA-PTX NAs; moreover, the extent of inhibition of FA-PTX NAs + anti-PD-1 was dramatically higher than that of NS + anti-PD-1 and FA NAs + anti-PD-1. There was no significant difference between the FA NAs+anti-PD-1 and NS + anti-PD-1 groups. Compared to NS or FA NAs, FA-PTX NAs displayed a greater degree of tumor growth inhibition, but not significantly so. The tumor weight in each group was recorded on day 21 after administration. As illustrated in *Figure 6C*, the average tumor weight in the FA-PTX NAs + anti-PD-1, FA NAs + anti-PD-1, NS + anti-PD-1, FA-PTX NA, NS, and FA NA groups was 0.47±0.14, 0.93±0.21, 0.99±0.19, 1.73±0.20, 1.83±0.18, and 1.95±0.16 g, respectively. As shown in *Figure 6D*, the body weights of mice in each group were similar. In addition, after 35 days of administration,

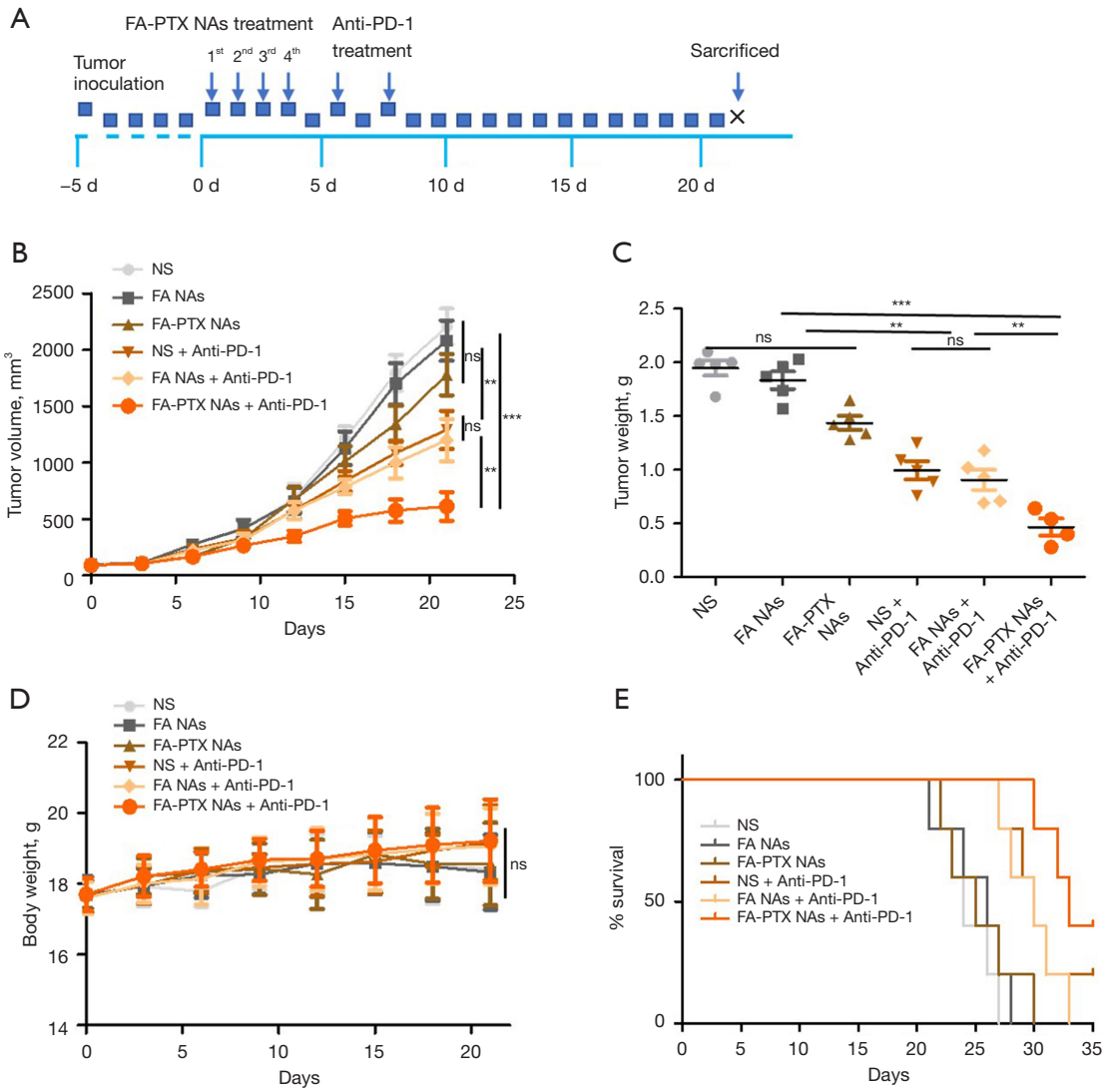

Figure 6 Antitumor effect of FA-PTX NAs on LLC cells *in vivo*. (A) Schematic diagram of the inoculation and treatment schedule. (B) Tumor volume growth curve, (C) tumor weights, (D) body weight, and (E) the survival curve of mice in each group. **, P<0.01; ***, P<0.001; ns, no significance. FA-PTX NA, folic acid-modified nanoassemblies loaded with paclitaxel; FA NA, folic acid-modified nanoassemblies; LLC, Lewis lung carcinoma; PD-1, programmed cell death protein-1.

although NS + anti-PD-1 and FA NAs + anti-PD-1 treatment improved the survival time, FA-PTX NAs + anti-PD-1 demonstrated a longer survival time (*Figure 6E*). These results suggest that FA-PTX NAs + anti-PD-1 has a higher antitumor efficacy against LLC than does FA NAs + anti-PD-1 or NS + anti-PD-1.

Antitumor mechanism and side effects

To clarify the underlying mechanisms for improving the response to ICIs of FA-PTX NAs *in vivo*, TUNEL, $CD4^+$ T-cell, $CD8^+$ T-cell, and HE staining were conducted. HE staining of tumor sections suggested that tumor tissues treated with FA-PTX NA or FA-PTX NAs + anti-PD-1 showed fewer blood vessels, and a combination of FA-PTX NAs and anti–PD-1 treatment increase the number of dead cancer cells. In contrast, there were more red blood cells and vessels in tumors treated with NS, FA NA, NS + anti-PD-1, and FA NAs + anti-PD-1 (*Figure 7A*). As shown in *Figure 7B*, tumor tissues treated with NS + anti-PD-1,

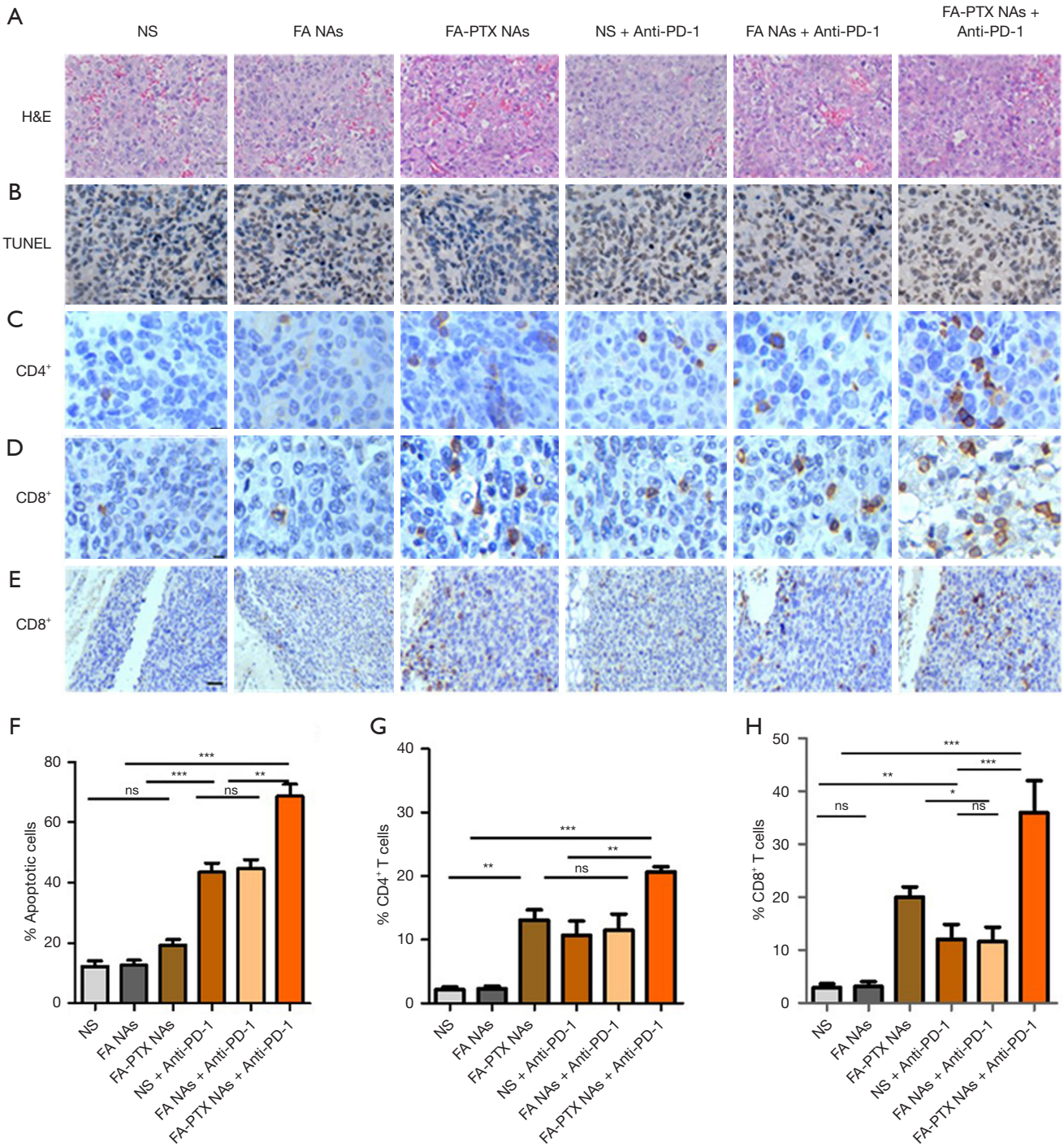

Figure 7 Antitumor mechanism analysis. (A) HE staining of tumor tissues. Scale bar =100 μm. (B) The apoptosis induction as determined by TUNEL assay. Scale bar =50 μm. (C) The number of $CD4^+$ and (D) $CD8^+$ T cells in tumors detected by IHC. Scale bar =50 μm. (E) The distribution of $CD8^+$ T cells in tumors detected by IHC. Scale bar =100 μm. (F-H) Tumor cell apoptosis and the abundance of $CD4^+$ T cells and $CD8^+$ T cells were assessed by counting the rate of TUNEL-positive cells and the number of $CD4^+$ and $CD8^+$ T cells, respectively. *, P<0.05; **, P<0.01; ***, P<0.001; ns, no significance. FA NA, folic acid-modified nanoassemblies; FA-PTX NA, folic acid-modified nanoassemblies loaded with paclitaxel; HE, hematoxylin and eosin; IHC, immunohistochemistry; NS, normal saline; PD-1, programmed cell death protein-1; TUNEL, terminal deoxynucleotidyl transferase 2'-deoxyuridine 5'-triphosphate nick end labeling.

FA NAs + anti-PD-1, and FA-PTX NAs + anti-PD-1 all had more TUNEL-positive tumor cells than did those treated with NA, FA NAs, or FA-PTX NAs NS. FA-PTX NAs + anti-PD-1 induced remarkable cell apoptosis when compared with NS + anti-PD-1 or FA NAs + anti-PD-1. In addition, the number of infiltrating $CD4^+$ and $CD8^+$ T cells in tumors assessed by IHC staining was markedly increased under treatment of FA-PTX NAs, NS + anti-PD-1, FA NAs + anti-PD-1, and FA-PTX NAs + anti-PD-1 as compared to treatment with NS and FA NAs. In contrast, a greater abundance of $CD4^+$ and $CD8^+$ T cells in tumors was observed in mice treated with FA-PTX NAs and FA-PTX NAs + anti-PD-1 than in those treated with NS + anti-PD-1 and FA NAs + anti-PD-1 (*Figure 7C*,*7D*). As can be seen in *Figure 7E*, there was large abundance of infiltrating $CD8^+$ T cells and distribution among tumor cells in tumors treated with FA-PTX NAs and FA-PTX NAs + anti-PD-1; meanwhile, under treatment with NS + anti-PD-1 and FA NAs + anti-PD-1, the infiltration of $CD8^+$ T cells was mainly distributed at the edge of tumors. Immunohistochemical scoring showed that the proportions of TUNEL-positive cells, $CD4^+$ T cells, and $CD8^+$ T cells in the FA-PTX NAs + anti-PD-1 treatment group were significantly higher than those in the other treatment groups (*Figure 7F-7H*). These results thus suggest that PTX can promote the infiltration and distribution of $CD4^+$ and $CD8^+$ T cells in the TIME, which are involved in the improvement of response to ICIs.

We also evaluated the safety of the combination treatment of FA-PTX NAs and anti-PD-1 through HE staining and cytokine detection. we found that there were no significant pathological changes in the lungs, liver, spleen, kidneys, or heart of mice treated with FA-PTX NAs combined anti-PD-1 (*Figure 8A*). Moreover, there were no significant differences in the levels of cytokines such as IL-2, IL-6, IL-8, IL-10, and TNF-α among the various treatment groups (*Figure 8B-8F*). These suggested that FA-PTX NA had no obvious side effects in mice.

Discussion

In this study, low-dosage PTX-enhanced NAs, FA-PTX NAs, were designed as a novel immunomodulator to improve the response to ICIs in lung cancer treatment. NAs loading with a low dose of PTX can significantly reprogram the immunosuppressive tumor microenvironment. Treatment with FA-PTX NAs combined with ICIs exerted synergistic effects in inhibiting lung cancer growth *in vivo*.

Immune tolerance of the tumor microenvironment remains the most significant challenge for cancer immunotherapy. The efficacy of ICI treatment is closely associated with the composition, function, and spatial location of immune cells within the TME, which composes the TIME (6,32). Considerable effort has been exerted to abolish the local immune tolerance of TIMEs in order to increase sensitization to ICI treatment. For instance, chemotherapy, radiation therapy, and small-molecule inhibitors have been developed to induce the immunogenic death of tumor cells and sensitize tumors to ICI therapy via the instigation of $CD8^+$ T-cell infiltration in the TIME (33-39). TGF-β signaling plays a vital role in excluding infiltrating T cells within the TIME, resulting in resistance to ICI treatment. Treatments blocking TGF-β signaling also contribute to improving the response to ICIs by inhibiting the exclusion of immune cells (30,40,41). A study by Mathios *et al.*, indicated that local chemotherapy could also be an effective strategy to breaking the immune tolerance of TIME, as it may facilitate the infiltration of tumor-associated DCs and the expansion of antigen-specific T effector cells; however, they found that systemic chemotherapy resulted in systemic and intratumoral lymphodepletion (42). Another strategy involves lowering the concentrations of chemotherapeutics because this can modulate the intratumoral cytokine network and lung cancer growth. In a study by Zhong *et al.*, low-dose PTX did not show any indication of inducing tumor resistance in a mouse lung cancer model (13). The tumor-specific immune response triggered by immunogenic cell death (ICD) induced by high-dose chemotherapy is also an important strategy for breaking the immune tolerance in the tumor microenvironment. However, this strategy may also be associated with severe toxic reactions and induce the apoptosis of immune cells. More importantly, its localization efficiency in the tumor microenvironment is relatively low. In recent years, stimuli-responsive multifunctional nanoparticles or nanocomposites carrying immunogenic cell death inducers have provided a promising solution for breaking the immunosuppressive tumor microenvironment (43).

Nanotechnology has been used to target the TIME and increase sensitization to immunotherapy. This involve the ability to program the location, pharmacokinetics, and delivery of immunomodulatory compounds acting on cells at target sites to elicit responses that cannot be achieved with the administration of such compounds in solution. For example, Li *et al.* prepared a nanocomplex composed of C-X-C motif chemokine receptor 4 (CXCR4) inhibitor

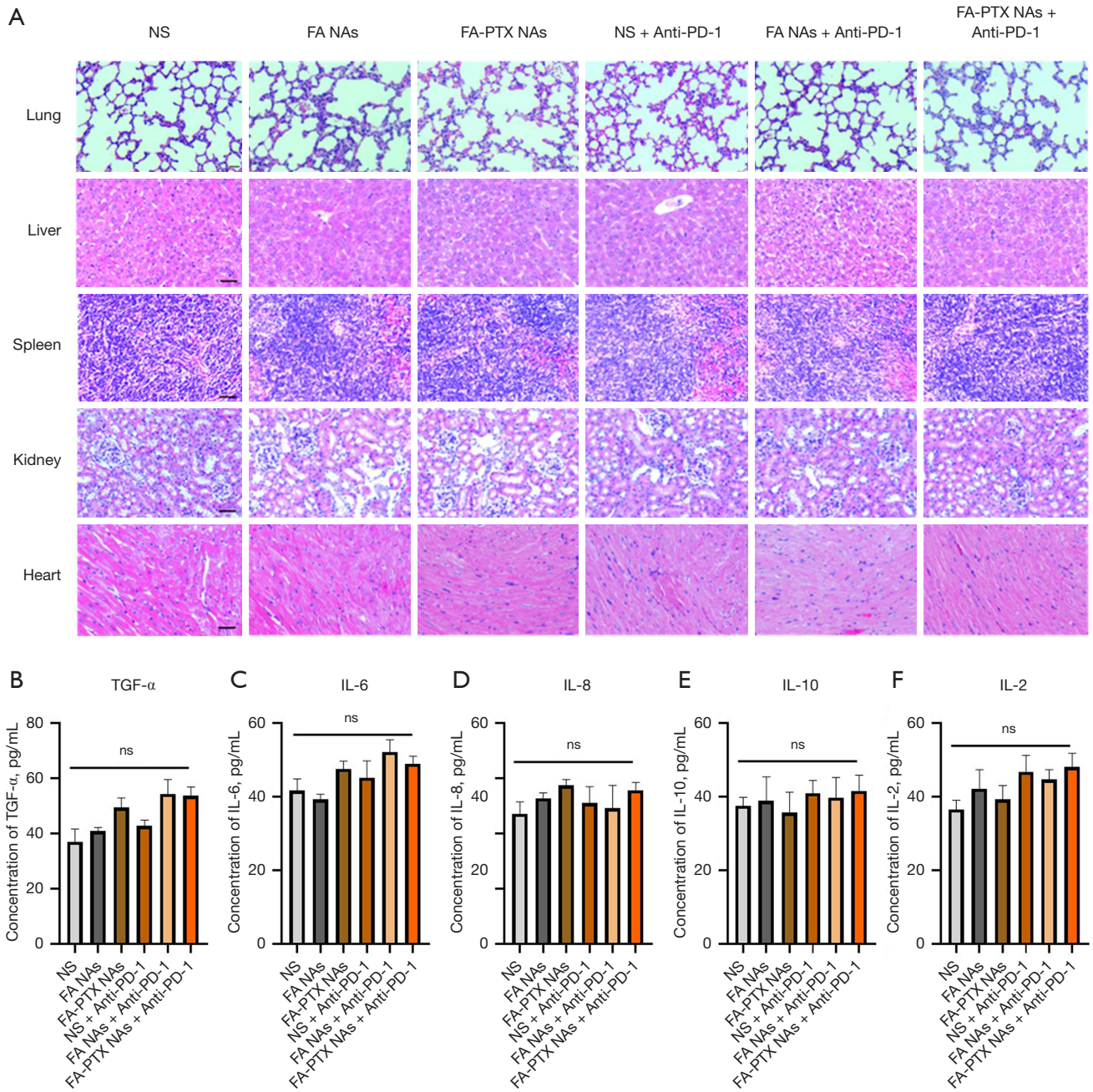

Figure 8 System toxicity evaluation. (A) Representative histological sections of vital organs stained with HE. Scale bar =100 μm. (B-F) The levels of serum cytokines were measured by ELISA. ns, no significance. ELISA, enzyme-linked immunosorbent assay; FA NA, folic acid-modified nanoassemblies; FA-PTX NA, folic acid-modified nanoassemblies loaded with paclitaxel; HE, hematoxylin and eosin; IL-6, interleukin-6; IL-8, interleukin-8; IL-10, interleukin-10; IL-2, interleukin-2; NS, normal saline; PD-1, programmed cell death protein-1; TNF-α, tumor necrosis factor-α.

and PTX to target the TME. The results showed that the complex induced T-cell infiltration and reduced the number of myeloid-derived suppressor cells and T regulatory cells in the tumor microenvironment, and enhanced the antitumor effects of immunotherapy (44). Tang *et al.* prepared PTX-loaded nanoparticles that could be effectively phagocytosed by macrophages and which polarized macrophages toward the M1 type and inhibited their differentiation both on the phenotypic and functional levels, consequently awakening the immune system to fight against cancer. Moreover, the PTX-loaded nanoparticles showed lower cytotoxicity toward BMDMs than did free PTX (12). Finally, Wen *et al.* found that macrophages highly express folate receptors (27), which is conducive to the targeted uptake of the prepared folic acid-modified nanoparticles by macrophages.

In our study, we leveraged coassembling to develop novel folic acid-modified low-dose PTX-loaded NAs, named *FA-PTX NAs*, to be used as immunomodulators to sensitize cancer cells to immunotherapy. The prepared FA-PTX NAs showed high drug encapsulation efficiency, good drug release profiles, good blood biocompatibility, a uniform size, and a weak negative zeta potential. The FA-PTX NAs were confirmed to be uptaken effectively by DCs, to promote the activation of DCs without obvious cytotoxicity *in vitro*, and to have a good targeting effect on the TIME *in vivo*. Given that the immune state of TIME is spatiotemporally controlled, therapies that influence the immune state of TIME should also be spatiotemporally controlled. Thus, we examined the dynamic changes in the immune state of the TIME caused by FA-PTX NAs to identify the optimal time window for immunotherapy and dose of PTX. The results showed that the improvement in TIME by FA-PTX NAs was dose- and time-dependent. This indicates that immunomodulators should require a certain time window in sensitizing immunotherapy to achieve the best synergistic antitumor effect. Subsequent experiments showed that FA-PTX NAs in combination with ICIs could efficiently inhibit the growth of lung cancer, showing potential applications in lung cancer immunotherapy. Our results indicate that combining PTX-enhanced nanoparticles with ICI treatment could be a new strategy for cancer immunotherapy with a synergistic antitumor effect and no significant cytotoxicity. This strategy has also inspired the design of a combined therapy of chemotherapeutic drug and immunotherapy.

However, certain limitations to this study should be acknowledged. Most notably, due to constraints such as time and research funding, we were unable to further explore the underlying mechanisms of how low-dose PTC activates DCs. This will be examined further in our subsequent work.

Conclusions

In this study, we demonstrated that low-dose PX-enhanced NAs can act as an immunomodulator for cancer immunotherapy. The immunosuppressive TIME was significantly improved by PTX-enhanced NAs. NAs loaded with low-dose PTX exerted a synergistic antitumor effect with immunotherapy. ICIs could more efficiently inhibit the growth of lung cancer cells, which were sensitized by the PTX-enhanced NAs, through apoptosis induction, $CD8^+$ T-cell infiltration increase, and the improved distribution of infiltrated $CD8^+$ T cells, thus supporting the application of NAs in lung cancer immunotherapy.

Acknowledgments

None.

Footnote

Reporting Checklist: The authors have completed the ARRIVE and MDAR reporting checklists. Available at https://tlcr.amegroups.com/article/view/10.21037/tlcr-2025-180/rc

Data Sharing Statement: Available at https://tlcr.amegroups.com/article/view/10.21037/tlcr-2025-180/dss

Peer Review File: Available at https://tlcr.amegroups.com/article/view/10.21037/tlcr-2025-180/prf

Funding: This work was supported by the Natural Science Foundation of Chongqing City (No. cstc2019jcyj-msxmX0614), the Sichuan Provincial Regional Innovation Cooperation Plan (No. 2022YFQ0004), and the Senior Medical Talents Program of Chongqing for Young and Middle-aged (No. 2020GDRC005).

Conflicts of Interest: All authors have completed the ICMJE uniform disclosure form (available at https://tlcr.amegroups.com/article/view/10.21037/tlcr-2025-180/coif). The authors have no conflicts of interest to declare.

Ethical Statement: The authors are accountable for all

aspects of the work in ensuring that questions related to the accuracy or integrity of any part of the work are appropriately investigated and resolved. All animals were cared for in accordance with the guidelines outlined in the Guide for the *Care and Use of Laboratory Animals*, *8th edition*. The animal experiments were approved and supervised by the Institutional Animal Care and Treatment Committee of the Chongqing University Cancer Hospital.

References

1. Sung H, Ferlay J, Siegel RL, et al. Global Cancer Statistics 2020: GLOBOCAN Estimates of Incidence and Mortality Worldwide for 36 Cancers in 185 Countries. CA Cancer J Clin 2021;71:209-49.
2. Paz-Ares L, Luft A, Vicente D, et al. Pembrolizumab plus Chemotherapy for Squamous Non-Small-Cell Lung Cancer. N Engl J Med 2018;379:2040-51.
3. Gadgeel S, Rodríguez-Abreu D, Speranza G, et al. Updated Analysis From KEYNOTE-189: Pembrolizumab or Placebo Plus Pemetrexed and Platinum for Previously Untreated Metastatic Nonsquamous Non-Small-Cell Lung Cancer. J Clin Oncol 2020;38:1505-17.
4. Li MSC, Mok KKS, Mok TSK. Developments in targeted therapy & immunotherapy-how non-small cell lung cancer management will change in the next decade: a narrative review. Ann Transl Med 2023;11:358.
5. Brahmer JR, Govindan R, Anders RA, et al. The Society for Immunotherapy of Cancer consensus statement on immunotherapy for the treatment of non-small cell lung cancer (NSCLC). J Immunother Cancer 2018;6:75.
6. Luo W, Wen T, Qu X. Tumor immune microenvironment-based therapies in pancreatic ductal adenocarcinoma: time to update the concept. J Exp Clin Cancer Res 2024;43:8.
7. Spranger S. Mechanisms of tumor escape in the context of the T-cell-inflamed and the non-T-cell-inflamed tumor microenvironment. Int Immunol 2016;28:383-91.
8. Meric-Bernstam F, Larkin J, Tabernero J, et al. Enhancing anti-tumour efficacy with immunotherapy combinations. Lancet 2021;397:1010-22.
9. Hotchkiss KM, Batich KA, Mohan A, et al. Dendritic cell vaccine trials in gliomas: Untangling the lines. Neuro Oncol 2023;25:1752-62.
10. Jhunjhunwala S, Hammer C, Delamarre L. Antigen presentation in cancer: insights into tumour immunogenicity and immune evasion. Nat Rev Cancer 2021;21:298-312.
11. Javeed A, Ashraf M, Riaz A, et al. Paclitaxel and immune system. Eur J Pharm Sci 2009;38:283-90.
12. Tang W, Yang J, Yuan Y, et al. Paclitaxel nanoparticle awakens immune system to fight against cancer. Nanoscale 2017;9:6529-36.
13. Zhong H, Han B, Tourkova IL, et al. Low-dose paclitaxel prior to intratumoral dendritic cell vaccine modulates intratumoral cytokine network and lung cancer growth. Clin Cancer Res 2007;13:5455-62.
14. Wang M, Herbst RS, Boshoff C. Toward personalized treatment approaches for non-small-cell lung cancer. Nat Med 2021;27:1345-56.
15. Liu X, Cheng Y, Mu Y, et al. Diverse drug delivery systems for the enhancement of cancer immunotherapy: an overview. Front Immunol 2024;15:1328145.
16. Chen Y, Zhou Q, Jia Z, et al. Enhancing cancer immunotherapy: Nanotechnology-mediated immunotherapy overcoming immunosuppression. Acta Pharm Sin B 2024;14:3834-54.
17. Huang L, Yang J, Wang T, et al. Engineering of small-molecule lipidic prodrugs as novel nanomedicines for enhanced drug delivery. J Nanobiotechnology 2022;20:49.
18. Ren G, Jiang M, Xue P, et al. A unique highly hydrophobic anticancer prodrug self-assembled nanomedicine for cancer therapy. Nanomedicine 2016;12:2273-82.
19. Kang T, Li Y, Wang Y, et al. Modular Engineering of Targeted Dual-Drug Nanoassemblies for Cancer Chemoimmunotherapy. ACS Appl Mater Interfaces 2019;11:36371-82.
20. Sun L, Li Z, Lan J, et al. Better together: nanoscale co-delivery systems of therapeutic agents for high-performance cancer therapy. Front Pharmacol 2024;15:1389922.
21. Sun B, Luo C, Cui W, et al. Chemotherapy agent-unsaturated fatty acid prodrugs and prodrug-nanoplatforms for cancer chemotherapy. J Control Release 2017;264:145-59.
22. Pei Q, Jiang B, Hao D, et al. Self-assembled nanoformulations of paclitaxel for enhanced cancer

theranostics. Acta Pharm Sin B 2023;13:3252-76.
23. Khan H, Shahab U, Alshammari A, et al. Nano-therapeutics: The upcoming nanomedicine to treat cancer. IUBMB Life 2024;76:468-84.
24. Khan H, Waseem M, Faisal M, et al. Inhibitory Effect of Multimodal Nanoassemblies against Glycative and Oxidative Stress in Cancer and Glycation Animal Models. Biomed Res Int 2021;2021:8892156.
25. Alenazi F, Saleem M, Syed Khaja AS, et al. Antiglycation potential of plant based TiO(2) nanoparticle in D-ribose glycated BSA in vitro. Cell Biochem Funct 2022;40:784-96.
26. Jing Z, Wang S, Xu K, et al. A Potent Micron Neoantigen Tumor Vaccine GP-Neoantigen Induces Robust Antitumor Activity in Multiple Tumor Models. Adv Sci (Weinh) 2022;9:e2201496.
27. Wen X, Shi C, Yang L, et al. A radioiodinated FR-β-targeted tracer with improved pharmacokinetics through modification with an albumin binder for imaging of macrophages in AS and NAFL. Eur J Nucl Med Mol Imaging 2022;49:503-16.
28. Pfannenstiel LW, Lam SS, Emens LA, et al. Paclitaxel enhances early dendritic cell maturation and function through TLR4 signaling in mice. Cell Immunol 2010;263:79-87.
29. Byrd-Leifer CA, Block EF, Takeda K, et al. The role of MyD88 and TLR4 in the LPS-mimetic activity of Taxol. Eur J Immunol 2001;31:2448-57.
30. Mariathasan S, Turley SJ, Nickles D, et al. TGFβ attenuates tumour response to PD-L1 blockade by contributing to exclusion of T cells. Nature 2018;554:544-8.
31. Wang Z, Wang B, Feng Y, et al. Targeting tumor-associated macrophage-derived CD74 improves efficacy of neoadjuvant chemotherapy in combination with PD-1 blockade for cervical cancer. J Immunother Cancer 2024;12:e009024.
32. Zhan X, Feng S, Zhou X, et al. Immunotherapy response and microenvironment provide biomarkers of immunotherapy options for patients with lung adenocarcinoma. Front Genet 2022;13:1047435.
33. Pfirschke C, Engblom C, Rickelt S, et al. Immunogenic Chemotherapy Sensitizes Tumors to Checkpoint Blockade Therapy. Immunity 2016;44:343-54.
34. Sharabi AB, Lim M, DeWeese TL, et al. Radiation and checkpoint blockade immunotherapy: radiosensitisation and potential mechanisms of synergy. Lancet Oncol 2015;16:e498-509.
35. Darragh LB, Oweida AJ, Karam SD. Overcoming Resistance to Combination Radiation-Immunotherapy: A Focus on Contributing Pathways Within the Tumor Microenvironment. Front Immunol 2018;9:3154.
36. Zhang Z, Liu X, Chen D, et al. Radiotherapy combined with immunotherapy: the dawn of cancer treatment. Signal Transduct Target Ther 2022;7:258.
37. Zhang T, Zhang C, Fu Z, et al. Immune Modulatory Effects of Molecularly Targeted Therapy and Its Repurposed Usage in Cancer Immunotherapy. Pharmaceutics 2022;14:1768.
38. Tong J, Tan X, Song X, et al. CDK4/6 Inhibition Suppresses p73 Phosphorylation and Activates DR5 to Potentiate Chemotherapy and Immune Checkpoint Blockade. Cancer Res 2022;82:1340-52.
39. Liu P, Zhao L, Pol J, et al. Crizotinib-induced immunogenic cell death in non-small cell lung cancer. Nat Commun 2019;10:1486.
40. Tauriello DVF, Palomo-Ponce S, Stork D, et al. TGFβ drives immune evasion in genetically reconstituted colon cancer metastasis. Nature 2018;554:538-43.
41. Chen SY, Mamai O, Akhurst RJ. TGFβ: Signaling Blockade for Cancer Immunotherapy. Annu Rev Cancer Biol 2022;6:123-46.
42. Mathios D, Kim JE, Mangraviti A, et al. Anti-PD-1 antitumor immunity is enhanced by local and abrogated by systemic chemotherapy in GBM. Sci Transl Med 2016;8:370ra180.
43. Xu W, Liu W, Yang J, et al. Stimuli-responsive nanodelivery systems for amplifying immunogenic cell death in cancer immunotherapy. Immunol Rev 2024;321:181-98.
44. Li Z, Wang Y, Shen Y, et al. Targeting pulmonary tumor microenvironment with CXCR4-inhibiting nanocomplex to enhance anti-PD-L1 immunotherapy. Sci Adv 2020;6:eaaz9240.

Cite this article as: Long J, Li D, Zhao W, Liang G, Huang L, Lei S, Li Y. Nanoassemblies loaded with low-dose paclitaxel can enhance the response of lung cancer immunotherapy by activating dendritic cells. Transl Lung Cancer Res 2025;14(4):1418-1440. doi: 10.21037/tlcr-2025-180